Tectonophysics 643 (2015) 80–93

Contents lists available at ScienceDirect

Tectonophysics

journal homepage: www.elsevier.com/locate/tecto

Cenozoic low temperature cooling history of the Northern Tethyan Himalaya in Zedang, SE Tibet and its implications

Guangwei Li [a,*], Yuntao Tian [b], Barry P. Kohn [a], Mike Sandiford [a], Zhiqin Xu [c], Zhihui Cai [c]

[a] School of Earth Sciences, University of Melbourne, Victoria 3010, Australia
[b] Department of Earth Sciences, University College London, London, United Kingdom
[c] State Laboratory for Continental Tectonics and Dynamics, Institute of Geology, Chinese Academy of Geological Sciences, Beijing 100037, China

ARTICLE INFO

Article history:
Received 27 August 2014
Received in revised form 22 December 2014
Accepted 28 December 2014
Available online 8 January 2015

Keywords:
Low temperature thermochronology
Cooling history
Tethyan Himalaya
Tibetan Plateau

ABSTRACT

Major structures and climatic change during the Cenozoic (especially Miocene) interacted to shape the giant Tibetan Plateau, whose formation was triggered by convergence of Indian and Asian plates. In this work, we report a low-temperature thermochronology data set from the northern Tethyan Himalaya and Indus–Yarlung suture zone in the Zedang area, where structures are defined by two parallel thrusts (the Zhongba–Gyantse Thrust to the south and Great Counter Thrust to the north). Eighteen samples from the region constrain their low temperature cooling and exhumation histories and further elucidate the evolution of the southern Tibetan Plateau. Thermal history modelling reveals Eocene and Miocene cooling episodes. Based on the temporal and spatial patterns, Eocene cooling is probably linked to crustal thickening resulting in the Eocene anatexis in the northern Tethyan Himalaya; the rapid pronounced cooling episode between ca. 20 Ma and 15 Ma in the Luobusha area reflects the activity of the Great Counter Thrust (GCT); the ca. 14–10 Ma cooling event of the Yardoi dome can probably be linked to rapid erosional denudation during that period; and pronounced cooling commencing in the middle Miocene was probably caused by incision of branches of the Yarlung–Zangbo River. A further cooling episode commencing in late Miocene time (ca. 5 Ma) in Luobusha area and Yardoi dome, may reflect initial activity of the Cona Graben cutting through the region.

1. Introduction

The northward motion of the Indian plate resulted in the Indian–Asian collision during the Cenozoic, and the subsequent uplift of the Himalayas, with important implications for global climate (e.g. Harrison et al., 1995; Molnar et al., 1993). Although many studies have been conducted to understand the formation of the plateau, several studies on its evolution in time and space, still remain much debated (e.g. Harrison et al., 1995; Tapponnier et al., 2001; Wang et al., 2008; Rohrmann et al., 2012; references therein). Low temperature thermochronology (e.g. apatite fission track and apatite/zircon U–Th/He dating) has been widely applied as a powerful tool for revealing the cooling/denudation/uplift history of Tibetan Plateau. However, most of this work has focused on the marginal regions of the Plateau (e.g. Burbank et al., 2003; Jolivet et al., 1999, 2001; Sobel et al., 2011; Tian et al., 2013, 2014 and references therein).

Some recent studies have begun to focus on the inner parts of the Tibetan Plateau. Multi-thermochronological data reported by Wang et al. (2008), Hetzel et al. (2011) and Rohrmann et al. (2012), revealed a rapid late Cretaceous–Early Eocene (between ~80 and 50 Ma) exhumation at a rate of ~300 m/m.y in central Tibet, followed by a phase of slow exhumation to the present day. The slow exhumation has been interpreted as evidence for formation of a flat topography (Hetzel et al., 2011) or the central Tibetan Plateau itself (Rohrmann et al., 2012). Two studies in the Gangdese batholith, located in the southern Lhasa terrane (Fig. 1), revealed a phase of enhanced Miocene cooling/exhumation (Copeland et al., 1995; Dai et al., 2013). Carrapa et al. (2014) reported an episode of Miocene exhumation of the Indus–Yarlung suture zone. Further south, Wang et al. (2010) documented middle Miocene and Late Miocene–Quaternary cooling episodes from the Greater Himalaya. Other studies have been conducted on major structures, such as the Great Counter Thrust (GCT) and the Southern Tibet Detachment system (STDS), the Main Central Thrust (MCT) and the W–E extension system (e.g. Edwards and Harrison, 1997; Harrison et al., 1995, 2000; Lee et al., 2011; Quidelleur et al., 1997; Stockli et al., 2002; Yin and Harrison, 2000). However, few studies have systematically investigated the denudation and uplift of the Tethyan Himalaya between the Lhasa terrane and the Greater Himalaya, located in the highest structural position within the Himalayan orogeny in south Tibet (Hodges, 2000). Major structures, such as the GCT, the Tethyan Himalayan fold–thrust system and the Northern Himalayan Gneiss domes, developed in this terrane (e.g. Quidelleur et al., 1997; Lee et al., 2000;

* Corresponding author at: School of Earth Sciences, University of Melbourne, McCoy Building, Corner Swanston & Elgin Streets, Parkville, Victoria 3010, Australia. Tel.: +61 3 90357571; fax: +61 3 83447761.
E-mail address: guangwei.li@unimelb.edu.au (G. Li).

http://dx.doi.org/10.1016/j.tecto.2014.12.014
0040-1951/

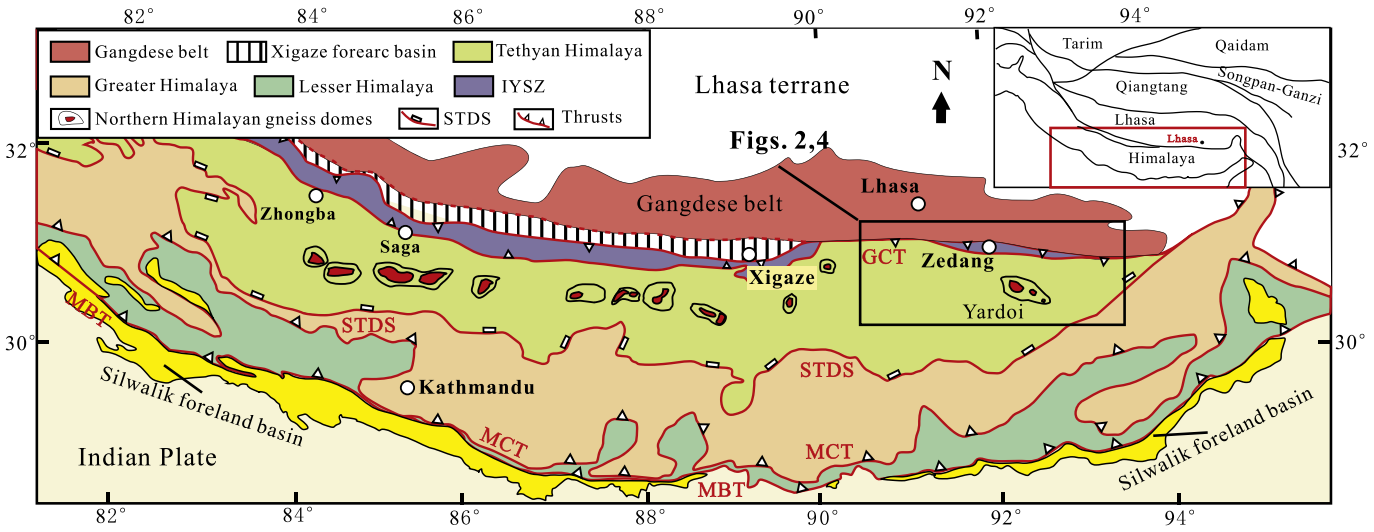

Fig. 1. Simplified tectonic map of Himalayan orogenic belt, south Tibet (modified after Ding et al., 2005). GCT, Great Counter Thrust; STDS, South Tibet Detachment system; MCT, Main Central Thrust; MBT, Main Boundary Thrust.

Yin, 2006), and record significant information on the evolution of southern Tibet Plateau since the India–Asia collision. Dunkl et al. (2011) reported vitrinite reflectance, K–Ar dating of illite as well as five zircon/apatite U–Th/He results in the region. These provided some understanding of the degree and age of metamorphism of the Triassic flysch sequence, but do not provide tight constraints on the post collisional cooling history. Here, we report apatite fission track (AFT) and zircon and apatite U–Th/He (AHe and ZHe) data principally from two N–S traverses in the northern Tethyan Himalaya to better reveal its cooling/exhumation history in the context of the regional India/Asia collision.

2. Geological setting

The southern Tibetan Plateau comprises several main units, the Lhasa terrane, the Indus–Yarlung suture zone, the Himalayas (including the Tethyan Himalaya, the Greater Himalaya, the Lesser Himalaya), which are separated by the Great Counter Thrust (GCT), the Southern Tibet Detachment system (STDS), The Main central thrust (MCT) and the Main Boundary thrust (MBT) (e.g. Burg and Chen, 1984; Yin and Harrison, 2000; references therein; Fig. 1). The southern Lhasa terrane is defined by a belt of igneous rocks, termed the Gangdese belt and represents an active Mesozoic–Cenozoic continental margin arc (Chu et al., 2006; Yin and Harrison, 2000; Zhu et al., 2013). Yin et al. (1994, 1999) suggested that the Gangdese belt is bounded by the Gangdese thrust to the south, however, the existence of the thrust was questioned by Aitchison et al. (2003).

The Indus–Yarlung suture zone (IYSZ), located to the south of the Gangdese belt and the Indus–Yarlung suture zone, represents remnants of the Neo-Tethys oceanic basin, which marks the boundary between the Indian and Asian continents (Burg and Chen, 1984; Yin and Harrison, 2000). It is locally defined by a north-directed thrust system referred to as the Miocene Great Counter Thrust (GCT) (Yin et al., 1999) and consists of late Jurassic to early Cretaceous ophiolitic and island arc volcanic rocks (Aitchison et al., 2000; Dubois-Côté et al., 2005; Malpas et al., 2003), as well as the Paleogene to/or Eocene–Miocene Liuqu conglomerate (Davis et al., 2002; Fang et al., 2006; Wei et al., 2011). The Tethyan Himalaya is separated by GCT and STDS and is composed of Paleozoic–Cenozoic sequences, which are widely considered as representing Indian passive continental margin deposits (Liu and Einsele, 1994). Cropping out within these rocks are the Northern Himalayan Gneiss domes consisting of Cambrian–Ordovician medium to high-grade metamorphic rocks that are intruded by 44–13 Ma leucogranites (e.g. Chen et al., 1990; Lee et al., 2000; Zeng et al., 2011; Zhang et al., 2012; Fig. 1). The formation of these domes has been linked to the diapirism of the granite generated by depression due to the extension of STDS (Zhang et al., 2012), but some may also have been generated by regional east–west extension (Guo et al., 2008). Additionally, the Tethyan Himalayan fold–thrust system developed in this belt during Eocene–Oligocene (Ratschbacher et al., 1994). The Greater Himalayan Sequence (GHS) between the MCT and SDTS consists of high-grade metamorphic rocks. The Lesser Himalayan is bounded by MCT and MBT and includes low-grade metamorphic Proterozoic–Cambrian sequences (Yin and Harrison, 2000). A widely developed north–south trending graben system in the region, has been active since the Miocene, indicating an E–W extensional regime (e.g. Harrison et al., 1995; Lee et al., 2011; Zhang et al., 2012; references therein).

The region studied is located in the Zedang area, in southeast Tibet (Figs. 1, 2), where a mainly Late Triassic flysch thrust-fold belt forming a synclinorium is exposed over a belt some 10–50 km wide, and is confined by the GCT to the north and the Eocene Zhongba–Gyantse Thrust (ZGT) to the south (Ding et al., 2005). This late Triassic turbidite sequence is a unique unit in the region and is regarded as part of the Indian continental margin (Liu and Einsele, 1994). However, several lines of evidence suggest that the sediment was probably derived from the Lhasa terrane and deposited on the southern margin of Lhasa terrane (Li et al., 2010, 2014). The Oligocene–Miocene Yardoi Gneiss dome intrudes the southern part of the turbidite sequence; discrete Cenozoic gabbro, diabase and diorite dykes or veins penetrate this belt and the late and post-Miocene Cona graben extends in a NS direction, adjacent to the east side of the Yardoi dome (Wu et al., 2008; Dunkl et al., 2011; Zeng et al., 2011; Figs. 2 and 3). The Luobusha–Zedang ophiolite zone, the eastern part of the IYSZ, is located to the north of the Late-Triassic sequences, and consists mainly of peridotites with podiform chromitites, gabbros and dolerite dikes, middle–late Cretaceous sandstone, phyllite, and a radiolarian chert mélange (Li et al., 2012; Fig. 2). In the northeast part of the studied region (Luobusha), the ophiolite mélange overthrusts the Oligocene–Lower Miocene Luobusha conglomerate along a north-directed shear zone, the Renbu–Zedang thrusts (parts of GCT, Quidelleur et al., 1997; Harrison et al., 2000; Fig. 2). Field observations and scientific drilling in the Luobusha area reveal that the Luobusha conglomerate unconformably overlies the undeformed Gangdese granite (Xu et al., 2015; Fig. 2).

3. Tectonic deformation in Zedang area

The intensely deformed late Triassic flysch sequence thrusting over the Zedang ophiolite zone along its northern boundary

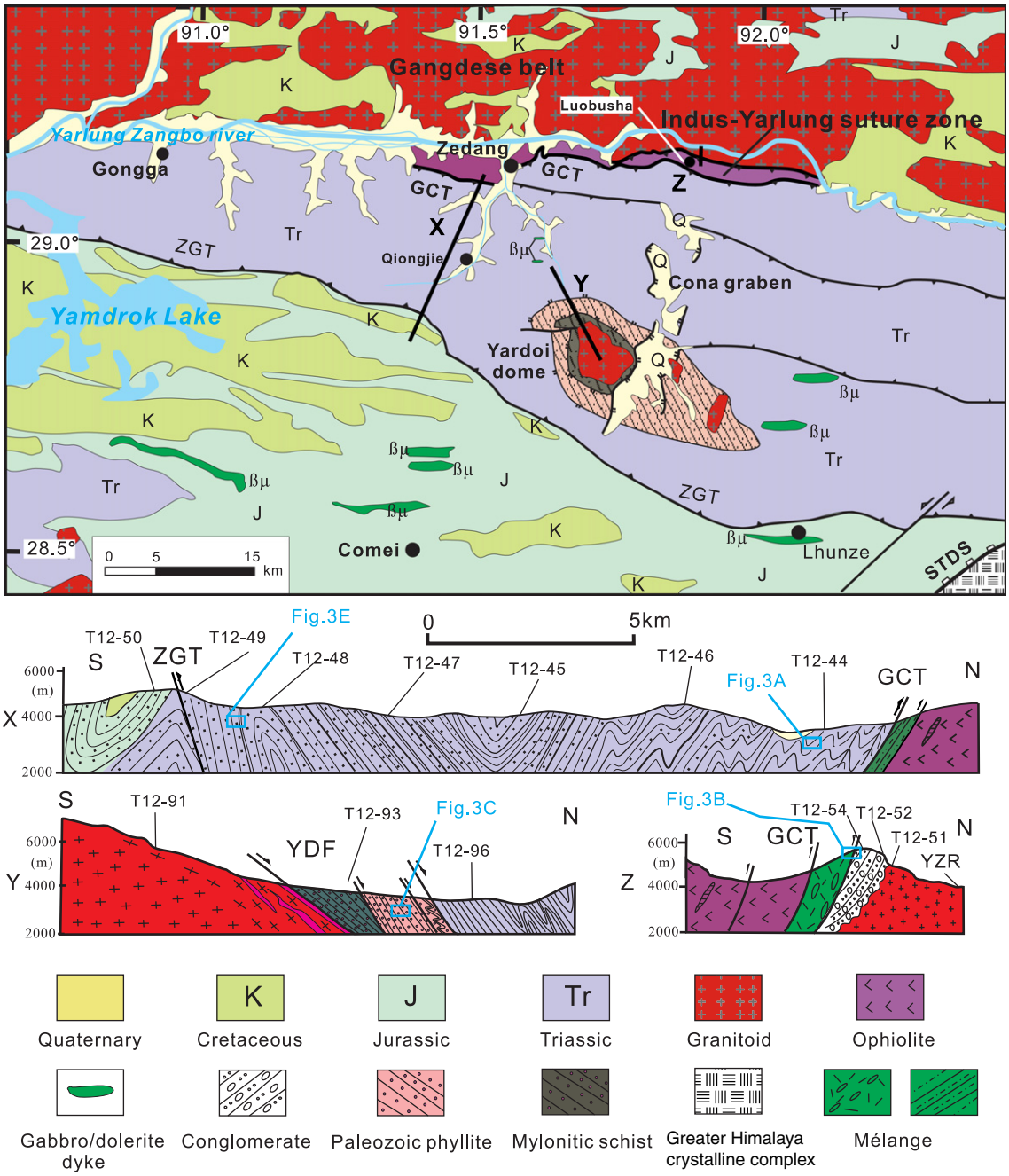

Fig. 2. Geological map and cross sections of Zedang area, southeast Tibet (modified from BGMRXAR, 1993). It includes: 'X' section through the late Triassic sequences; 'Y' section through the northern part of the Yardoi dome area; 'Z' section through the Luobusha area. GCT, Great Counter Thrust; IYSZ, Indus–Yarlung Suture Zone; STDS, South Tibet Detachment system; YDF, Yardoi detachment faults; YZR, Yarlung–Zangbo River.

experienced low-grade (anchi- to epizonal) metamorphism (Dunkl et al., 2011). Structures, including penetrative foliation, tight folds with gently south-dipping axial planes, drag folds, quartz veins with σ-type rotational mortar textures, S/C fabrics, and south-dipping imbricate thrusts, suggest a top-to-the north sense of shear (Fig. 3A). These superimposed structures represent at least two phases of deformation (Dunkl et al., 2011; Xu et al., 2015). The central part of this sequence reveals a synclinal core with vertical penetrative cleavage, while the southern part shows relatively weaker deformation, containing many tight folds with north-dipping axial planes and some recumbent folds (Fig. 3E), formed by the regional N–S contraction. Tethyan Himalayan Jurassic sediments are situated in the footwall of the ZGT (BGMRXAR, 1993; Ding et al., 2005). The Yardoi gneiss dome exposes a Cenozoic granite pluton in the core and three lithologic–tectonic units separated by the NNW-Yardoi detachment faults (YDF) active at least at ~14 Ma as determined by muscovite Ar–Ar dating of the mylonitic leucogranite (Zhang et al., 2012). These include a lower unit of schist and garnet-bearing gneiss, a middle unit of deformed phyllite and schist with σ-type porphyroclasts indicating top-down-to-NNW sliding (Figs. 2, 3C) and an upper part with low-grade metamorphosed Triassic flysch (Fig. 2; Zhang et al., 2012). In addition, in the Luobusha area the GCT (locally termed the Renbu–Zedang thrust) is represented by a mylonitic mélange suite with mylonitic foliation planes, quartz ribbons, σ-type feldspar porphyroclasts indicating top-to-north shearing (Fig. 3B, D), which was active from ~19–15 Ma (Quidelleur et al., 1997).

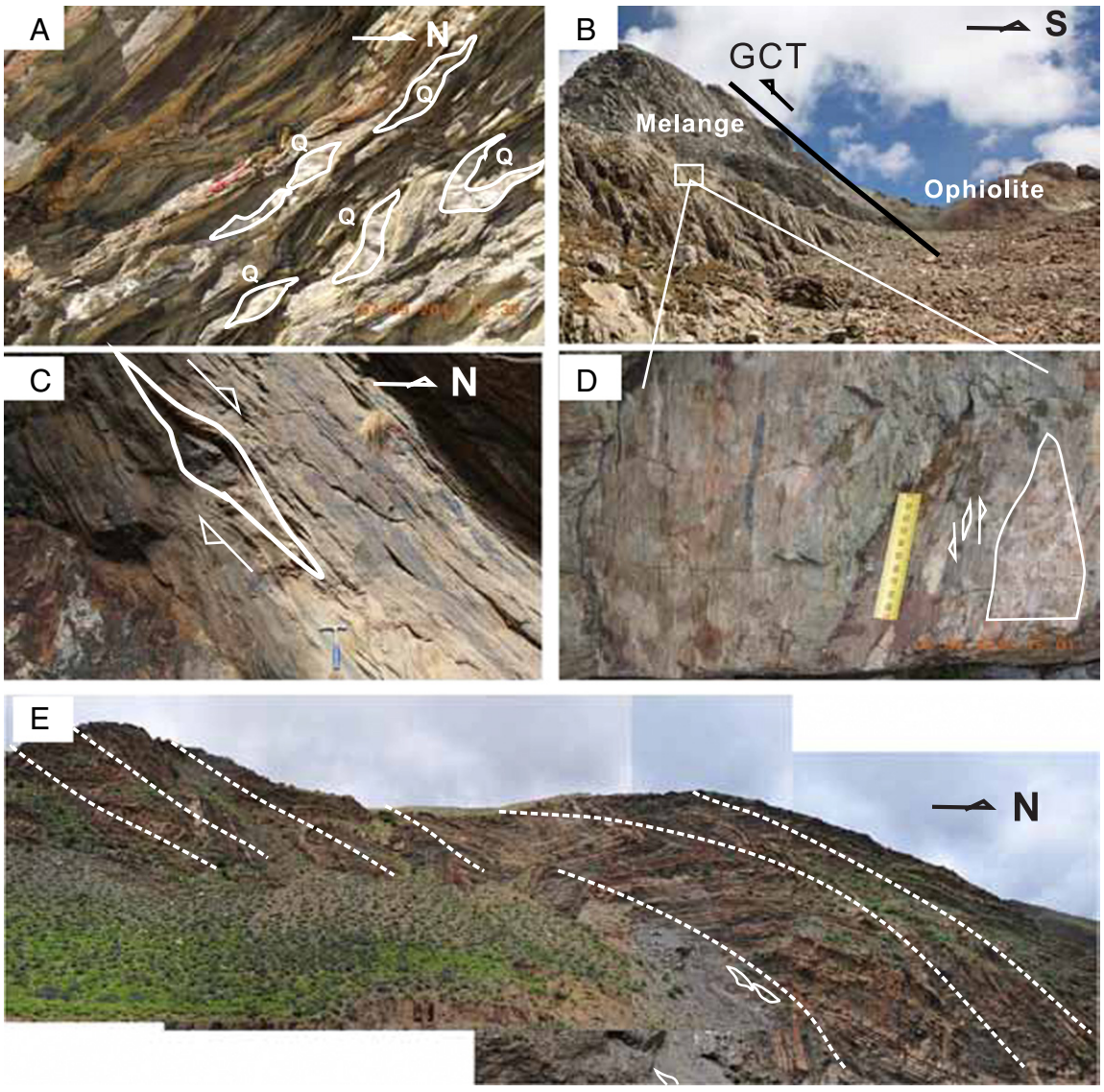

Fig. 3. Rocks and structures in the Zedang area. (A) Northern part of late Triassic slate with S–C and sigma indicators showing top-to-north thrusting (GCT); (B) Zedang ophiolite northward thrusting over mélange; (C) gneiss of the Yardoi dome with sigma indicators, indicating top-down-to-NNW sliding (northwestern side of the dome); (D) mylonite shown in photo B (Great Counter Thrust in Luobusha area); (E) southern part of the late Triassic sequence with folds showing south-ward thrusting. White dashed lines represent the axial planes.

4. Samples and methods

Twelve samples were collected from Tethyan Himalayan sandstone along two principal N–S transects (A–A′, B–B′) crosscutting the GCT and ZGT and a shorter section (C–C′) in the Zedang area, including one sample (T12-50) from Jurassic sandstone in the footwall of ZGT (Figs. 2, 4). Along transect B-B′, one meta-sandstone sample and two leucogranitic samples were also collected from the Yardoi dome (Fig. 4).

A further three samples (one granite T12-51, two sandstone T12-52, -54) were collected from the footwall of GCT in the Luobusha town (transect D–D′; ca. 150 km eastward from Zedang) (Figs. 2Z, 4). Sample T12-51 is from the late Cretaceous Gangdese granite (Quidelleur et al., 1997); while sandstone samples T12-52, and T12-54 were collected from the lower and upper parts of the Luobusha conglomerate, respectively (Fig. 2c). These samples are located on the south flank ridge of the Yarlung–Zangbo River valley (Figs. 2c, 4).

Following crushing and grinding, apatite and zircon grains were concentrated using standard heavy liquid and magnetic separation techniques. Apatite fission track (AFT), apatite (U–Th)/He (AHe) and zircon (U–Th)/He (ZHe) analyses were carried out on samples according to their mineral yields. Details of AHe and ZHe experimental methods follow those described by Tian et al. (2012, 2013), while those for AFT analysis are identical to those described by Tian et al. (2014), and are outlined briefly below. Grains were mounted in epoxy resin, ground and polished to an optical finish to expose internal grain surfaces. Mounts were etched in 5 M HNO_3 for 20 s at 20 °C to reveal fossil tracks. Apatite grains with polished surfaces parallel to prismatic crystal faces and homogeneous track distributions were selected and images taken using a Zeiss Axio Imager M1m microscope for counting tracks, and measuring horizontal confined track-lengths (HCTL) and etch pit diameters (Dpar). Where possible, fission tracks in at least 20 suitable apatite grains were counted and nearly 100 HCTL measured per sample. Only etched and HCTL were measured in grains with polished surfaces paralleling the *c*-axis. For all samples (see Table 1), ^{252}Cf tracks were implanted into polished grains to increase the number of confined track in tracks (TINTs) available for length measurement, thus providing a more robust data set for inverse thermal history

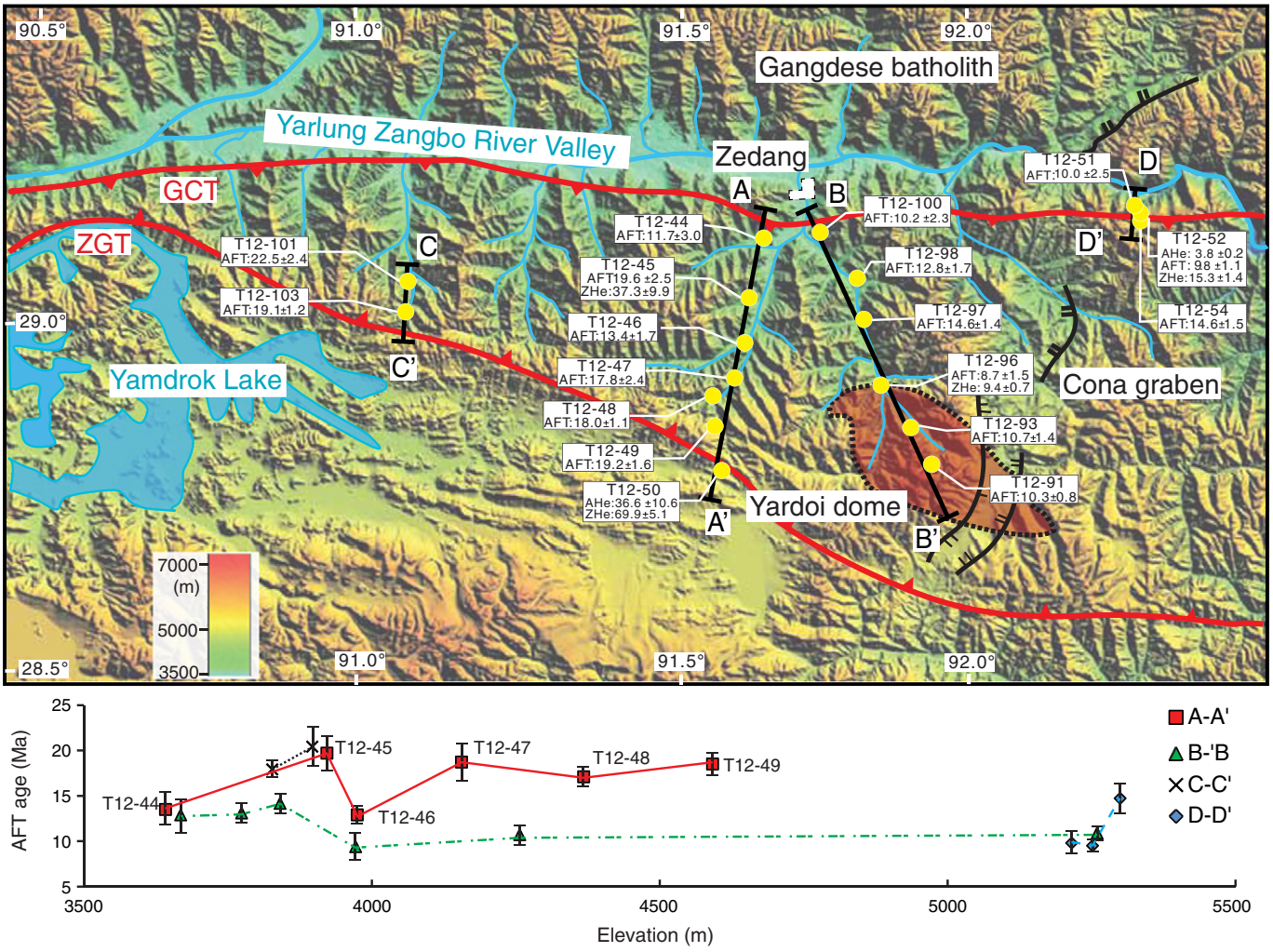

Fig. 4. Upper panel is a shaded relief map of the Zedang area showing major structures and drainage system, samples locations with the low-T thermal age data (white-filled square). These were taken along four sampling transects A–A′ to D–D′. Lower panel shows AFT age-elevation plots along sampling transects marked in the upper penal, and samples along transect A–A′ are labelled.

modelling. Uranium content of selected grains was determined using a LA-ICP-MS system using NIST 612 glass as a standard.

5. Results

AFT, AHe and ZHe ages of most samples, except for samples T12-52 and T12-54, are significantly younger than their host formation/stratigraphic ages (Tables 1, 2 and Fig. 3) and therefore considered to have been fully thermally reset. For those samples yielding both AHe and ZHe data, their AFT ages are consistently younger than their ZHe ages and older than their AHe ages. Although these samples were located at different elevations from 3600 to 5300 m, there is no significant correlation between their ages and elevation (Fig. 4).

5.1. AFT data

The Gangdese granite and Cenozoic sediments from the footwall of the GCT in the Luobusha town (transect D–D′) yield AFT pooled ages of 10.0 ± 2.1 Ma, 9.8 ± 1.1 Ma and 14.6 ± 1.5 Ma, respectively. Their non-projected track lengths are short, with similar mean values ranging between 10.0 ± 2.1–10.5 ± 3.7 μm (Table 1), indicating that they were reheated and have remained within the AFT partial annealing zone (60–110 °C) for a prolonged period prior to their exhumation to the surface (Gleadow et al., 1986).

AFT ages from eleven samples of Late Triassic sediments range between 11.7 ± 3.0 Ma and 22.5 ± 2.4 Ma (Table 1 and Figs. 5, 6). Most mean track lengths (MTL) for these samples range between 10.9 ± 2.0 and 11.4 ± 1.9 μm, except for T12-45, T12-98 and T12-103 with relatively longer MTL (12.2 ± 1.7, 13.0 ± 1.4 and 12.7 ± 1.6 μm). Those samples with short MTL may have remained within the AFT partial annealing zone for a long period prior to their later cooling. This possibility is consistent with the regional thermal history, which includes Cretaceous volcanic activity (Zhu et al., 2013) and Oligo-Miocene anchi- to epizonal metamorphism (Dunkl et al., 2011). Three samples (T12-45, -98, -103) with relatively longer MTL, may have experienced relatively faster exhumation after reheating (Gleadow et al., 1986). Samples T12-44 and T12-100 located near the GCT (Fig. 4), yield slightly younger apparent AFT ages. It is worth noting that apparent ages in transect A–A′ generally vary from anticline to syncline; sample T12-46 from the core of the synclinorium yields the youngest AFT age of 13.4 ± 1.7 Ma, while those from the north and south flanks are older (Figs. 2 and 4).

Three samples from the Yardoi dome along transect B–B′, yield concordant ages of 8.7 ± 1.5 Ma, 10.7 ± 1.4 Ma and 10.3 ± 0.8 Ma, with relatively long MTL (12.0 ± 2.1, 12.4 ± 1.5 μm and 12.8 ± 1.4 μm), indicating that they may have experienced faster exhumation following thermal resetting. No significant Dpar variation (mean values range from 1.40 to 1.81 μm) has been observed amongst the samples reported in this work (Table 1).

Table 1
Apatite fission track data, northern Tethyan Himalaya and IYSZ in Zedang area.

Sample no.	Collection information			Age results								Track length and Dpar results			Mean Dpar (range) (μm)
	Lithology	Locality (°E/°N)	Elevation (m)	No. of grains (n)	Spontaneous tracks		[a] Pooled ^{238}U (ppm)	[b] Pooled age (Ma ± 1SD)	[c] P(χ^2) (%)	Dispersion (%)	[d] Central age (Ma ± 1SD)	[e] Non-projected	[f] Projected	No. (n)	
					No. (n)	Density (10^5 cm^{-2})						Mean (μm ± 1SD)	Mean (μm ± 1SD)		
Luobusha (Gangdese belt)															
T12-51	Granite	92.300/29.198	5216	26	140	1.370	27.30	10.0 ± 2.1	83	10	10.7 ± 1.5	10.5 ± 3.7	12.9 ± 1.9	108	1.63 (1.3–1.8)
T12-52	Sandstone	92.298/29.198	5252	24	234	3.246	65.47	9.8 ± 1.1	24	12	10.4 ± 0.8	10.0 ± 2.1	12.3 ± 1.9	99	1.69 (1.0–1.9)
T12-54	Sandstone	92.299/29.195	5300	20	68	2.332	36.74	14.6 ± 1.5	33	10	15.7 ± 2.0	10.1 ± 2.2	12.5 ± 2.0	89	1.74 (1.4–2.2)
Late Triassic meta-sediments															
T12-44	Sandstone	91.712/29.124	3642	20	113	2.085	37.94	11.7 ± 3.0	32	13	14.7 ± 2.1	11.3 ± 1.8	12.8 ± 2.1	48	1.43 (1.2–1.8)
T12-45	Sandstone	91.659/28.964	3922	20	144	2.288	23.76	19.6 ± 2.5	24	25	21.5 ± 2.3	12.2 ± 1.7	13.4 ± 1.8	99	1.81 (1.3–2.1)
T12-46	Sandstone	91.691/29.050	3975	22	162	2.730	44.49	13.4 ± 1.7	60	5	14.1 ± 1.1	11.1 ± 1.9	12.7 ± 1.7	111	1.40 (1.3–1.6)
T12-47	Sandstone	91.618/28.909	4156	25	184	2.720	34.92	17.8 ± 2.4	38	20	20.5 ± 2.4	11.2 ± 2.0	13.0 ± 1.9	126	1.46 (1.0–2.0)
T12-48	Sandstone	91.632/28.879	4368	24	257	3.381	43.19	18.0 ± 1.1	28	15	18.4 ± 1.3	11.3 ± 2.1	12.9 ± 2.1	112	1.57 (1.2–2.0)
T12-49	Sandstone	91.646/28.836	4592	25	314	3.560	40.97	19.2 ± 1.6	20	18	20.3 ± 1.5	11.1 ± 1.8	13.0 ± 1.6	110	1.51 (1.2–2.1)
T12-97	Sandstone	91.878/29.016	3841	20	74	2.043	28.40	14.6 ± 1.4	35	12	15.4 ± 1.8	10.9 ± 2.0	12.7 ± 1.6	94	1.41 (1.1–1.7)
T12-98	Sandstone	91.871/29.066	3774	24	235	3.225	51.12	12.8 ± 1.7	54	29	14.4 ± 1.5	13.0 ± 1.4	13.7 ± 1.8	83	1.56 (1.4–1.9)
T12-100	Sandstone	91.820/29.125	3668	21	96	1.568	24.38	10.2 ± 2.3	48	24	14.2 ± 2.1	10.9 ± 2.1	12.8 ± 1.8	96	1.51 (1.1–1.9)
T12-101	Sandstone	91.108/29.100	3897	23	177	3.417	34.78	22.5 ± 2.4	63	12	22.3 ± 2.5	11.4 ± 1.9	12.9 ± 1.7	113	1.60 (1.1–2.1)
T12-103	Sandstone	91.111/29.127	3827	25	467	4.528	48.08	19.1 ± 1.2	13	5	19.6 ± 1.0	12.7 ± 1.6	13.6 ± 1.6	101	1.43 (1.1–1.7)
Yardoi dome															
T12-91	Granite	91.994/28.833	5260	31	406	1.568	28.68	10.3 ± 0.8	68	12	10.9 ± 0.8	12.8 ± 1.4	13.8 ± 1.3	107	1.63 (1.3–1.9)
T12-93	Granite	91.953/28.888	4257	25	135	1.441	27.04	10.7 ± 1.4	54	21	11.7 ± 1.2	12.4 ± 1.5	13.5 ± 1.6	95	1.42 (1.2–1.8)
T12-96	Schist	91.920/28.936	3972	22	103	1.858	41.15	8.7 ± 1.5	47	20	10.0 ± 1.2	12.0 ± 2.1	12.9 ± 1.8	74	1.47 (1.2–1.8)
FCT[g]	–	–	–	35	736	2.286	15.43	28.2 ± 2.0	68	8	29.1 ± 1.5	–	–	–	–
DUR[g]	–	–	–	20	276	1.600	9.80	32.5 ± 2.0	90	0	33.7 ± 2.1	–	–	–	–

[a] Pooled uranium content of all grains measured by LA-ICP-MS.
[b] Pooled AFT ages of all grains.
[c] P-value of χ^2 for (n − 1) degrees of freedom (Galbraith, 1981).
[d] Central age calculated using the RadialPlotter programme of Vermeesch (2009).
[e] Lengths measured after ^{252}Cf irradiation.
[f] *c*-axis projected mean track length after Ketcham et al. (2007).
[g] Apatite fission-track dating standards, with reference ages constrained by previous studies (McDowell et al., 2005; Bachmann et al., 2007).

Table 2
Results of zircon and apatite (U–Th)/He dating, northern Tethyan Himalaya and IYSZ in Zedang area.

Sample no.	No. of grains (n)	U ppm	Th ppm	Sm ppm	Th/U	[a][eU] ppm	[b]Mean FT	Gas ncc	Mass (mg)	[c]Grain radius (um)	Corr. age (Ma)	Error ± 1σ	[d]Weighted mean age (Ma ± 2σ)
Apatite													
T12-50	1	3.2	17.6	184.7	5.54	7.3	0.71	0.139	0.0045	83.0	47.9	2.1	
T12-50	2	1.7	9.5	171.6	5.67	3.9	0.76	0.069	0.0071	71.3	25.3	1.2	36.6 ± 10.6
T12-52	1	58.4	75.4	148.5	1.29	76.1	0.75	0.103	0.0040	62.2	3.7	0.2	
T12-52	2	6.8	25.3	74.4	3.74	12.7	0.77	0.037	0.0099	84.2	3.1	0.1	3.8 ± 0.2
T12-52	3	13.1	59.6	427.2	4.54	27.1	0.70	0.031	0.0025	60.4	5.4	0.2	
Zircon													
T12-45	1	425.4	128.6		0.30	455.6	0.75	8.714	0.0043	79.1	36.1	2.2	
T12-45	2	221.9	139.5		0.63	254.6	0.76	6.426	0.0059	86.8	35.3	2.2	37.3 ± 5.9
T12-45	3	206.4	125.7		0.61	235.9	0.76	6.213	0.0051	78.3	42.0	2.6	
T12-50	1	285.2	55.3		0.19	298.2	0.75	10.526	0.0040	77.2	71.3	4.4	
T12-50	2	200.2	189.9		0.95	244.8	0.74	10.337	0.0039	76.8	88.8	5.5	69.9 ± 5.1
T12-50	3	427.4	75.8		0.18	445.2	0.77	15.324	0.0047	82.0	60.1	3.7	
T12-52	1	324.0	261.0		0.81	385.3	0.77	4.385	0.0054	85.4	17.2	1.1	
T12-52	2	314.1	233.8		0.74	369.0	0.77	4.012	0.0064	89.5	14.0	0.9	15.3 ± 1.4
T12-96	1	195.2	113.7		0.58	221.9	0.74	1.232	0.0044	78.6	10.4	0.6	
T12-96	2	219.2	36.5		0.17	227.8	0.78	1.308	0.0059	88.0	8.2	0.5	9.4 ± 0.7
T12-96	3	192.4	60.1		0.31	206.5	0.78	1.929	0.0079	95.8	9.7	0.6	

[a] Effective uranium content, [eU] = [U] + 0.235 × [Th] (Flowers et al., 2009).
[b] α-Ejection correction (Farley et al., 1996) calculated using the individual radius.
[c] Radius of a sphere with the equivalent surface-area-to-volume ratio as cylindrical crystals (Meesters and Dunal, 2002).
[d] Weighted means at 95% confidence level calculated using Isoplot V3.25 (Ludwig, 2003).

5.2. AHe and ZHe data

AHe dating was conducted on two samples. Sample T12-50 from the southernmost Jurassic sandstone (transect A–A′) yielded two dispersed pre-Miocene ages. Sample T12-52 in transect D–D′ yielded reproducible Pliocene ages with a weighted average age of 3.8 ± 0.2 Ma (Table 2 and Fig. 3).

Four sandstones samples (T12-45, -50, -52 and -96) of different depositional ages (late Triassic, early Jurassic and late Oligocene–early Miocene, respectively) were selected for ZHe dating (Tables 1, 2 and Fig. 3). Samples T12-45, T12-52 and T12-96 yield reproducible Cenozoic ages from late Eocene to middle Miocene, with weighted means of 37.3 ± 5.9, 15.3 ± 1.4 and 9.4 ± 0.7 Ma, respectively (see Table 2). Sample T12-50 from the Jurassic sandstone yielded late Cretaceous ages with weighted mean average age of 69.9 ± 5.1 Ma (Table 2 and Fig. 4). Further, these ZHe ages are significantly younger than the depositional ages of their host strata, and therefore have been thermally reset totally with respect to ZHe thermochronometry (>180 °C, Reiners et al., 2004).

6. Thermal modelling and interpretations

6.1. Thermal modelling strategy for single samples

Combining AFT, AHe and ZHe data together with regional geological constraints, thermal history modelling for individual surface samples was carried out using the HeFTy software (Ketcham, 2005). In this study, AFT data are modelled using the multi-kinetic annealing model of Ketcham et al. (2007), with Dpar as a kinetic parameter; AHe data were modelled using the radiation damage accumulation and annealing model (RDAAM; Flowers et al., 2009); and ZHe data were modelled using the helium diffusion model of Guenthner et al. (2013).

Additional geological constraints taken into account in the thermal history modelling were as follows. (i) Present-day mean surface temperature of 10 ± 5 °C. (ii) An initial time–temperature constraint was set at 60–120 ± 10 °C at a time span older than the corresponding AFT age. (iii) Where applicable, broad temperature constraints of 40–80 °C and 160–200 °C were set around the time of the weighted mean AHe and ZHe ages. (vi) Depositional ages for samples (T12-52 and T12-54) from the Cenozoic Luobusha Formation (BGMXAR, 1993) were taken into consideration (Fig. 5). (vii) K-feldspar Ar–Ar ages from the GCT (Quidelleur et al., 1997) were used to constrain the modelling parameters for samples T12-51, -52, -54, which were collected from immediately beneath the fault zone.

The high temperature thermal histories of granitic samples T12-91 and T12-93 from Yardoi dome (Zhang et al., 2012) were constrained by their muscovite Ar–Ar ages. In HeFTy software, *c*-axis projected lengths were used for thermal modelling, and the modelling for each sample was conducted so as to obtain 100 'Good-Fit' paths (merit value: 0.5), and more than 1000 'Acceptable-Fit' paths (merit value: 0.05). All results are shown in Figs. 5 and 6. Furthermore, temporal information concerning the important inflection points in the model results for each sample is listed in Fig. 7.

6.2. Thermal history modelling results

6.2.1. Luobusha area (transect D–D′)

Thermal history modelling of the three samples all show a consistent thermal history post-ca. 20 Ma, which indicates that they experienced a pronounced cooling episode from ca. 20 Ma to ca. 15 Ma, then resided for around 10 Ma in the AFT partial annealing zone before undergoing a further rapid cooling episode at ca. 6–5 Ma (Fig. 5). The AHe, AFT and ZHe systems in sandstone samples T12-52 and T12-54, appear to have undergone thermal resetting shortly after their deposition (Fig. 5).

6.2.2. Late Triassic sediments (transects A–A′, B–B′ and C–C′)

Modelling of AFT data (some in combination with AHe and ZHe data) for 11 samples between the GCT and the ZGT yields a similar thermal history, which is characterised by relatively rapid cooling commencing in the middle and late Miocene (between ca. 15 and ca. 6 Ma) following residence for at least 10 Ma in the AFT partial annealing zone (see Figs. 5, 6 and 7). Considering their uncertainties, the Miocene cooling probably commenced between ca. 12 and 7 Ma (Fig. 7). Miocene cooling rates of samples T12-101 and T12-103 (transect C–C′) appear to be slightly lower. The cooling history for sample T12-45 suggests a rapid cooling history ending at ca. 35 Ma, followed by a later cooling episode from ca. 15 Ma (Figs. 6 and 7).

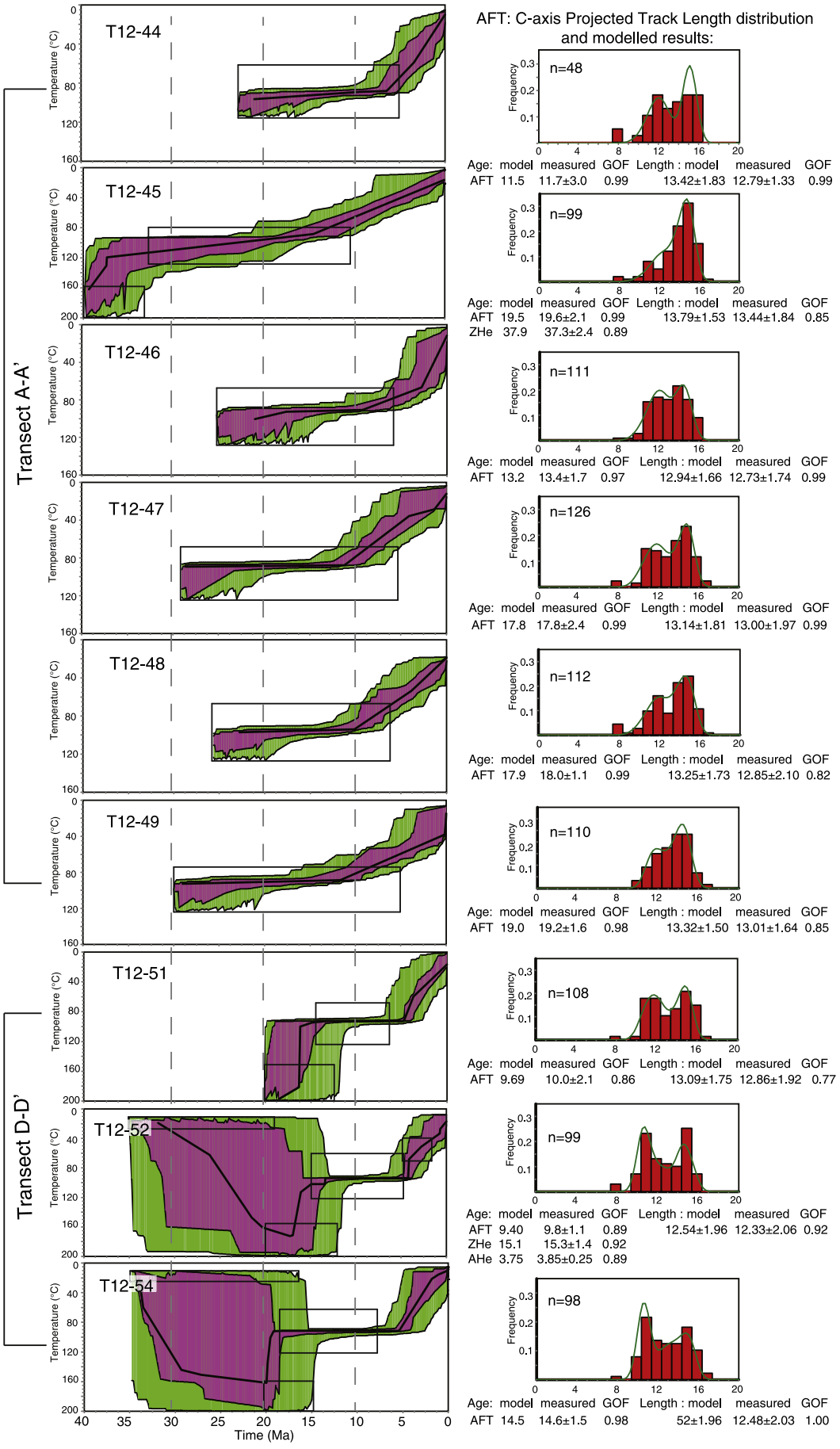
Transect A-A'
Transect D-D'
T12-44
T12-45
T12-46
T12-47
T12-48
T12-49
T12-51
T12-52
T12-54
Temperature (°C)
Time (Ma)
AFT: C-axis Projected Track Length distribution and modelled results:
n=48
Age: model measured GOF Length : model measured GOF
AFT 11.5 11.7±3.0 0.99 13.42±1.83 12.79±1.33 0.99
n=99
Age: model measured GOF Length : model measured GOF
AFT 19.5 19.6±2.1 0.99 13.79±1.53 13.44±1.84 0.85
ZHe 37.9 37.3±2.4 0.89
n=111
Age: model measured GOF Length : model measured GOF
AFT 13.2 13.4±1.7 0.97 12.94±1.66 12.73±1.74 0.99
n=126
Age: model measured GOF Length : model measured GOF
AFT 17.8 17.8±2.4 0.99 13.14±1.81 13.00±1.97 0.99
n=112
Age: model measured GOF Length : model measured GOF
AFT 17.9 18.0±1.1 0.99 13.25±1.73 12.85±2.10 0.82
n=110
Age: model measured GOF Length : model measured GOF
AFT 19.0 19.2±1.6 0.98 13.32±1.50 13.01±1.64 0.85
n=108
Age: model measured GOF Length : model measured GOF
AFT 9.69 10.0±2.1 0.86 13.09±1.75 12.86±1.92 0.77
n=99
Age: model measured GOF Length : model measured GOF
AFT 9.40 9.8±1.1 0.89 12.54±1.96 12.33±2.06 0.92
ZHe 15.1 15.3±1.4 0.92
AHe 3.75 3.85±0.25 0.89
n=98
Age: model measured GOF Length : model measured GOF
AFT 14.5 14.6±1.5 0.98 52±1.96 12.48±2.03 1.00
Frequency

6.2.3. Yardoi dome (transect B–B′)

Thermal history modelling for three samples (T12-91, T12-93 and T12-96) from the Yardoi dome indicates a recent two-stages cooling history with very rapid cooling between ca. 14 and 10 Ma, followed by a period of relative stability and accelerated cooling from ca. 5 Ma (Figs. 6, 7).

Generally, most samples studied show a relatively rapid cooling episode commencing in middle Miocene time (mainly ca. 12–8 Ma), while sample T12-45 with zircon He data also indicates a rapid cooling episode during Eocene time. Furthermore, samples from Luobusha (D–D′) display pronounced cooling between ca. 20 and 15 Ma (Figs. 5, 7), while those from the Yardoi dome show rapid cooling between ca. 14 and 10 Ma (Figs. 6, 7).

7. Discussion

7.1. Cooling history of Zedang area

Low temperature thermochronology ages reported in this study are all Cenozoic, except for sample T12-50 from Jurassic strata on the southern side of the ZGT, which yields a late Cretaceous ZHe age (Tables 1, 2). Most ages are less than 20 Ma, and mainly record the Miocene cooling/denudation history of the Zedang area in the late phase of the India/Asia collision. Our thermochronological data suggest that the Cenozoic cooling history is characterised by two main episodes of relatively rapid cooling and exhumation, one Eocene and another since the middle Miocene (Figs. 5, 6 and 7).

(1) Eocene cooling
This rapid cooling stage is only recorded by sample T12-45 (Figs. 5 and 7) by combining its ZHe and AFT data (Fig. 2). Noteworthy is that sample T12-50 from Jurassic sandstone with much older ZHe and AHe ages may possibly also record this cooling episode (Table 2). However, its detailed cooling history cannot be clearly elucidated without AFT data. This possible episode may have been related to the increased denudation during the regional uplift caused by crustal thickening in the Tethyan Himalaya, which is evidenced by Eocene anatexis in the Yardoi dome (Aikman et al., 2012; Zeng et al., 2011). Alternatively, it may not exclude the influence by the activity of the Tethyan Himalaya fold–thrust system around this time (Ding et al., 2005; Ratschbacher et al., 1994; Yin and Harrison, 2000) in the early stage of the India/Asian collision. Due to the continuing converge between Indian and Asian plates, a series of imbricated thrusts and anatexis developed in the Tethyan Himalaya during the Eocene (Yin and Harrison, 2000), resulting in the crustal thickening and uplift of the uppermost crust and this is probably recorded by the cooling episode evidenced by low temperature data in this area.

(2) Miocene cooling
In the Luobusha area, a rapid cooling episode between ca. 20 and 15 Ma probably reflects the activity of the GCT. As reported by Quidelleur et al. (1997), the GCT in this area experienced fault drag from ca. 19 to 15 Ma. Hence, it is probable that samples collected from the footwall of the GCT (Figs. 2, 3), underwent high temperature (>200 °C) reheating during the period of the activity of GCT, then at around ~15 Ma as fault activity waned, rapidly cooled to temperatures within the AFT partial annealing zone. Subsequently, rapid cooling recommenced in the latest Miocene (around ca. 6–5 Ma), probably resulting from the activity of the Cona Graben which cuts through the Yardoi dome and extends to the Luobusha area (Fig. 2; Dunkl et al., 2011).

For late Triassic sediments, the variable apparent AFT ages in transect A–A′, probably reflect differential exhumation and cooling during early deformation. The ages of samples from the northern and southern flanks are older than that of the synclinorium core, probably because the flanks were exhumed earlier from the partial annealing zone than rocks in the core of the syncline. The younger apparent AFT ages of the samples T12-44 and T12-100 probably present post-thrust cooling along the GCT. The Miocene cooling history shown by modelling (mainly by AFT data) of the late Triassic sediments indicates a phase of rapid cooling commencing in middle Miocene with timing of onsets from ca. 15 to 6 Ma (with most spanning ca. 12–8 Ma). However, considering the uncertainties involved in AFT modelling (Ketcham, 2005), we propose that the rapid cooling episode generally commenced in middle Miocene (see Fig. 7). As evidenced by the Miocene conglomerates along the Indus–Yarlung suture zone, the paleo-YZR was probably distributed along the Indus–Yarlung suture zone, cutting through the study area during/prio to the Miocene (DeCelles et al., 2007; Wang et al., 2013; references therein). Based on the analysis of the Himalayan foreland basin, Cina et al. (2009) proposed that the paleo-Yarlung–Zangbo River ran and incised through the study area during the Miocene time. Hence, the similarity in timing for onset of cooling probably indicates an erosional process along branches of YZR system in this area at that time. Cooling rates in samples across the section A–A′ and B–B′, are slightly higher than those from samples T12-101 and T12-103 in transect 'D–D' (Fig. 6), and this may be attributed to slightly different rates of river incision in the area (Fig. 4).

In the Yardoi dome, samples T12-91, -93, and -96 show slightly lower apparent AFT ages from ca. 10.3 ± 0.8 Ma to 8.7 ± 1.5 Ma between the dome centre and its northwestern flank (Fig. 4), which indicates that doming probably ceased before ca. 10 Ma. Because the continuously active domes usually yield low-T thermochronological ages younging from the margin to the core (Braun et al., 2014). This would be consistent with Ar–Ar data from the Yardoi dome indicating that doming had ceased by at least ca. 14 Ma (Zhang et al., 2012). The pronounced cooling episodes between ca. 14–10 Ma, can therefore probably be linked to post-doming erosional denudation of the Yardoi dome during that period. According to the local high topography and two river valleys cutting through the dome (Fig. 4), this rapid post-doming cooling/denudation was probably caused by local fluvial or glacial erosion. Later apparent cooling commencing at ca. 6–5 Ma (see Figs. 6, 7), probably resulted from the activity of the Cona Graben at that time as well. Combined with significant cooling commencing at around ca. 5 Ma in the Luobusha area, this may reflect a young episode of E–W extension in this area.

7.2. Tectonic implications

7.2.1. Implications for the evolution in south Tibet

The possible Eocene rapid cooling/denudation episode indicated by samples T12-45 and possibly T12-50, may reflect the crustal thickening in the Tethyan Himalaya, which is evidenced by Eocene anatexis in the Yardoi dome (Aikman et al., 2012; Zeng et al., 2011), and/or activity of the Tethyan Himalayan fold–thrust system (e.g. ZGT) during that time (Ding et al., 2005; Ratschbacher et al., 1994; Yin and Harrison, 2000).

Fig. 5. Thermal history modelling based on apatite fission track (AFT) and (U–Th–Sm)/He (AHe and ZHe) data using HeFTy (Ketcham, 2005) for samples from the Zedang area. Models use the AFT annealing model of Ketcham et al. (2007) and the radiation damage accumulation and annealing apatite/zircon He diffusion model (Flowers et al., 2009). Geological and low-T thermochronological constraints (see text for further details) are drawn as a black box. Left parts: purple envelopes indicate 'good' thermal paths GOF = goodness of fit (GOF > 0.55) and green envelopes indicate 'acceptable' thermal paths (GOF > 0.05). The best-fit thermal path for each sample is shown as a heavy black line. Right part: below the length distribution panel, the AFT and AHe modelled by the best-fit thermal path are compared with the measured data. Furthermore, results of modelling suggest a possible late Cenozoic episode of cooling (see text for further details). GOF, "good of fit".

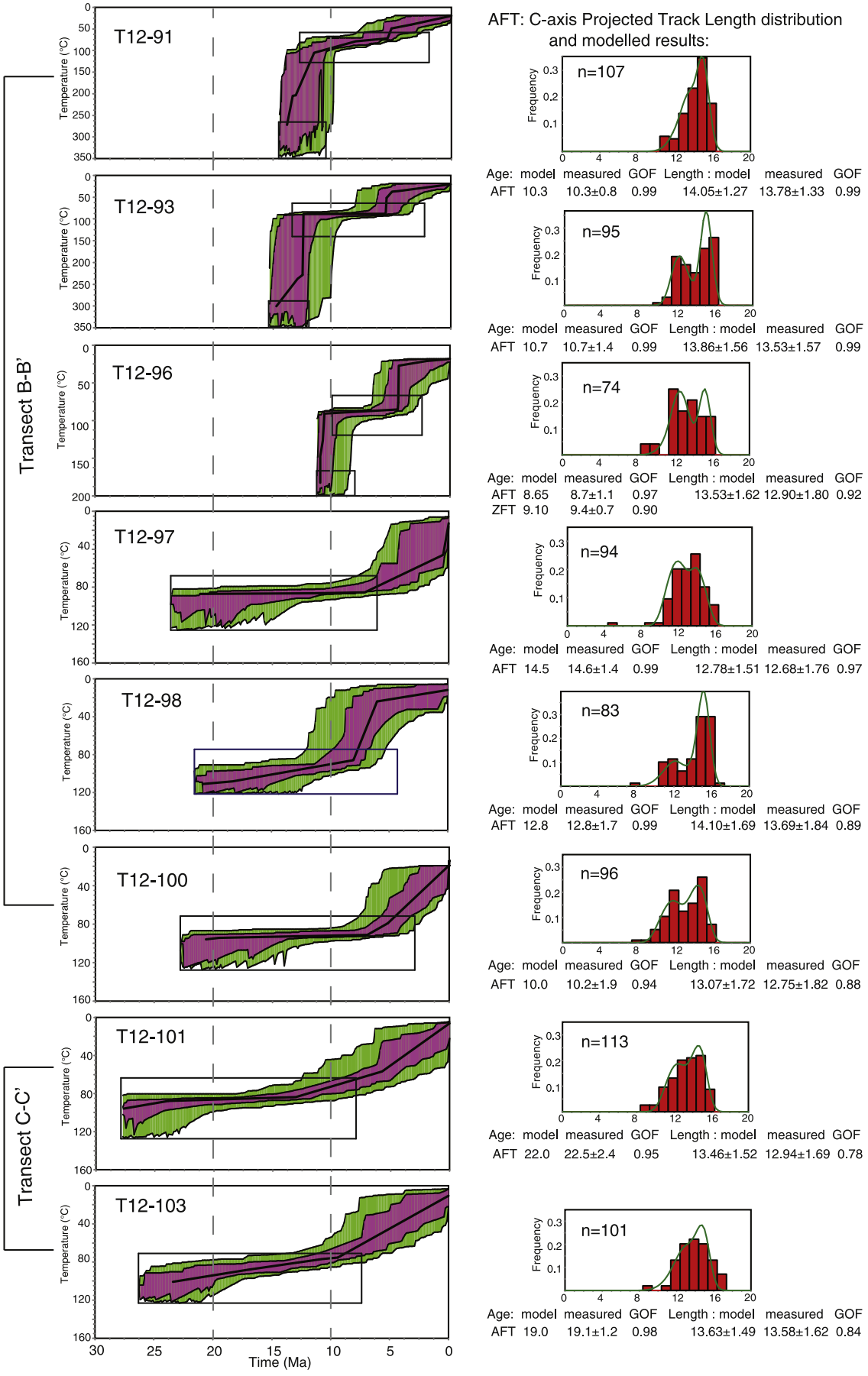
Transect B-B'
Transect C-C'
T12-91
T12-93
T12-96
T12-97
T12-98
T12-100
T12-101
T12-103
Temperature (°C)
Time (Ma)
AFT: C-axis Projected Track Length distribution and modelled results:
n=107
Age: model measured GOF Length : model measured GOF
AFT 10.3 10.3±0.8 0.99 14.05±1.27 13.78±1.33 0.99
n=95
Age: model measured GOF Length : model measured GOF
AFT 10.7 10.7±1.4 0.99 13.86±1.56 13.53±1.57 0.99
n=74
Age: model measured GOF Length : model measured GOF
AFT 8.65 8.7±1.1 0.97 13.53±1.62 12.90±1.80 0.92
ZFT 9.10 9.4±0.7 0.90
n=94
Age: model measured GOF Length : model measured GOF
AFT 14.5 14.6±1.4 0.99 12.78±1.51 12.68±1.76 0.97
n=83
Age: model measured GOF Length : model measured GOF
AFT 12.8 12.8±1.7 0.99 14.10±1.69 13.69±1.84 0.89
n=96
Age: model measured GOF Length : model measured GOF
AFT 10.0 10.2±1.9 0.94 13.07±1.72 12.75±1.82 0.88
n=113
Age: model measured GOF Length : model measured GOF
AFT 22.0 22.5±2.4 0.95 13.46±1.52 12.94±1.69 0.78
n=101
Age: model measured GOF Length : model measured GOF
AFT 19.0 19.1±1.2 0.98 13.63±1.49 13.58±1.62 0.84

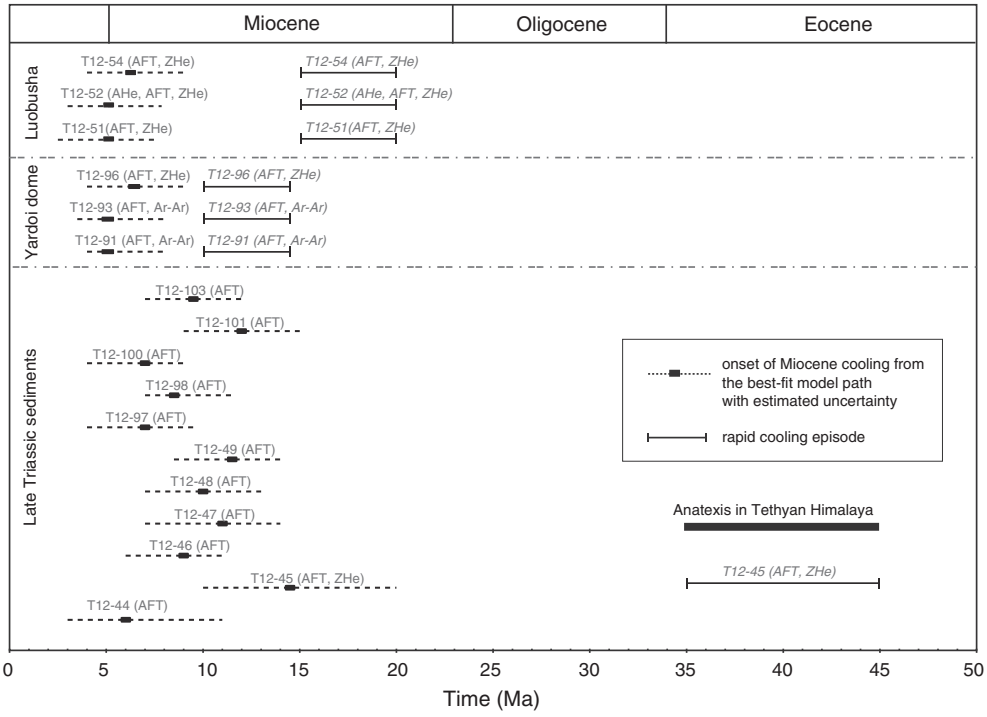

Fig. 7. Summary of the time of Cenozoic cooling episodes in the study area as calculated from thermal history modelling (see Figs. 5, 6). Onset of distinct Miocene cooling episode (black squares) is based on the time of inflections of best-fit thermal paths in models, while their uncertainty (dashed line) is calculated from the range of 'acceptable' thermal paths.

Samples in the Luobusha area, show an episode of rapid cooling between ca. 20 and 15 Ma, which probably signals early activity along the GCT. Rapid cooling commencing in middle Miocene in Zedang has implications for regional erosion caused by incision of the regional drainage system (Yarlung–Zangbo River, YZR) and the enhanced Asian monsoon (Nakayama and Ulak, 1999). The timing of this incision is comparable to that reported from branches of the YZR in the southern Lhasa terrane (Spicer et al., 2003). Generally, the time of onset of middle Miocene erosional cooling in the Zedang area is similar to that of nearby areas, for example, the Gangdese Batholith (an episode since ca. 11 Ma; Dai et al., 2013) to the north, Greater Himalaya (two episodes during middle Miocene and late Miocene–Pliocene; Wang et al., 2010) to the south (Fig. 8), which indicates enhanced erosion of the regional drainage system since the middle Miocene. Furthermore, the activity of the Cona Graben, shown by the identical rapid cooling commencing at ca. 5 Ma in the Luobusha and the Yardoi dome area (Figs. 5, 7). The middle Miocene accelerated erosion in south Tibet outlined above is supported by a contemporary increase of the oceanic $^{87}Sr/^{86}Sr$ ratio (Hodell and Woodruff, 1994; Hodell et al., 1991) and sedimentation rate in the Bengal Bay basin (Klootwijk et al., 1992).

7.2.2. Implications for the uplifting of Tibet Plateau

Previous paleoaltimetry studies suggest that the central Tibetan Plateau had uplifted to near-modern elevations by Eocene–Oligocene time (DeCelles et al., 2007; Ding et al., 2014; Quade et al., 2011; Rowley and Currie, 2006). Low-temperature thermochronological data, indicate that low erosion rates of <0.05 mm/yr in central Tibet were established by ca. 45 Ma and these are interpreted as a proxy for the establishment of regional low relief at high elevation (Hetzel et al., 2011; Rohrmann et al., 2012). Furthermore, recent studies of adakitic, ultrapotassic, and shoshonitic rocks in the Lhasa terrane suggest that crustal thickening caused uplift of the Lhasa terrane and that this occurred pre/during the Oligocene (Chung et al., 2009; Zhao et al., 2009). Collectively, most of central Tibet (mainly including the Qiangtang and Lhasa terrane) had at least formed a near-modern plateau by Oligocene time. In the Tethyan Himalaya, Eocene–Oligocene anatexis signifies that crustal thickening occurred during that time (Lee et al., 2000; Zeng et al., 2011; Zhang et al., 2012). The Tethyan Himalayan fold–thrust system was also initiated during the Eocene (Ding et al., 2005). Much of the new data presented here from the late-Triassic sequences in the northern Tethyan Himalaya, yield early-Miocene AFT ages (ca. 20–15 Ma), and these are consistent with the majority of AFT ages from the Gangdese batholith at a similar modern elevation (Copeland et al., 1995). This consistency between the AFT ages, demonstrating a regional-wide middle Miocene cooling episode (Fig. 8), probably suggests that these similar planation surfaces had formed in these two areas prior to the Miocene. This timing is also in accord with the proposal by Rohrmann et al. (2012) that the plateau had extended to the Tethyan Himalaya by ca. 23 Ma and to Greater Himalaya during the middle Miocene (Dai et al., 2013). Hence, the evidence above supports the proposition that the Plateau first developed as a central core prior to or during the Eocene and subsequently expanding radially towards the surrounding margins (Ding et al., 2014; Rohrmann et al., 2012; Wang et al., 2008).

To summarize, following the initial collision between Indian and Asian plates, the central Plateau reached high elevation and the Tethyan Himalayan fold–thrust system developed in south Tibet during Eocene time. Due to continuing convergence between the two plates, the Tibetan plateau had extended to the Tethyan Himalaya in the south and to the Hoh Xil in the north by Oligocene–early Miocene time (Wang et al., 2008). Simultaneously, major structures (e.g. GCT, STDS, MCT, and E–W extension system) developed in south Tibet (e.g. Edwards et al., 1996; Yin et al., 1999; Harrison et al., 2000; Xu et al., 2013; Fig. 8), concomitant with the strong crustal shortening in northern Tibet (Yin, 2006; Wang et al., 2008), while climate change in the

Fig. 6. Further results of thermal history modelling based on apatite fission track (AFT) and (U–Th–Sm)/He (AHe) data using HeFTy (Ketcham, 2005) for samples from the Zedang area using the AFT annealing model of Ketcham et al. (2007) and the radiation damage accumulation and annealing apatite He diffusion model (Flowers et al., 2009).

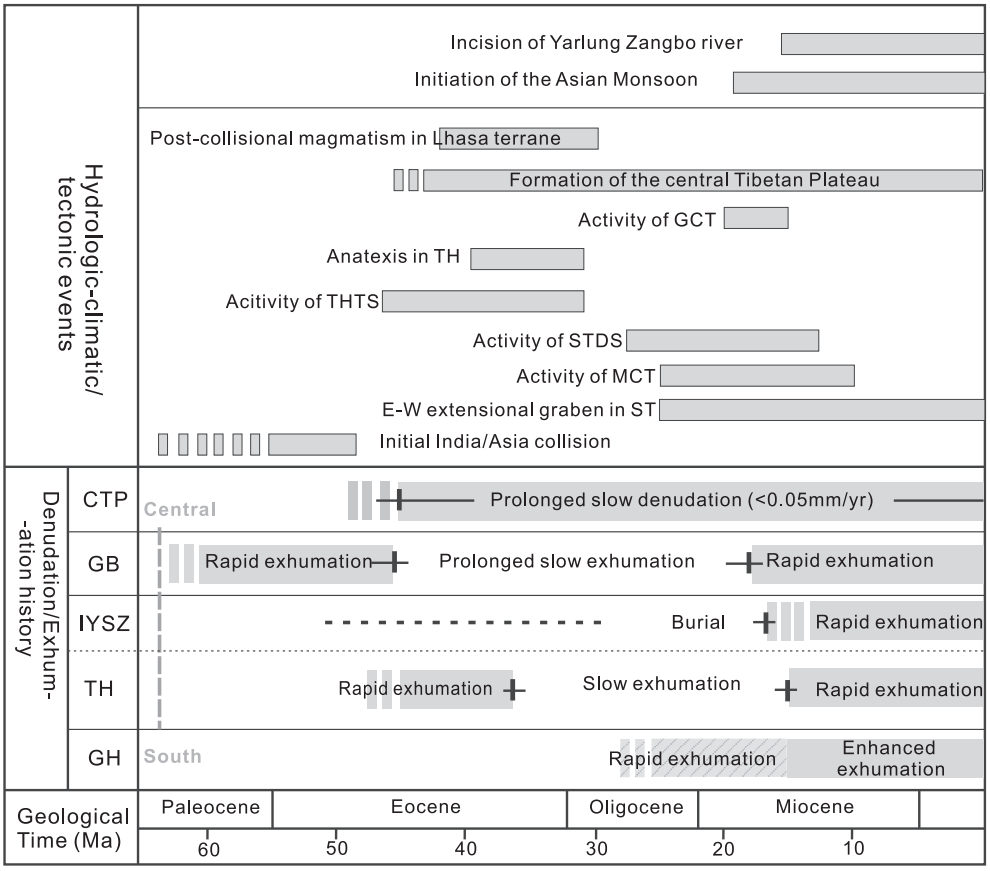

Fig. 8. Summary of the cooling/denudation history of units in southern Tibet, compared with the timing of other regional events: Incision of the Yarlung–Zangbo River in Lhasa terrane after Spicer et al. (2003), initiation of the Asian monsoon after Sun & Wang (2005), post-collisional magmatism in Lhasa terrane after Chung et al. (2009) and Zhao et al. (2009), formation of the central Tibetan Plateau after Rohrmann et al. (2012), activity of GCT, THTS, STDS, MCT after Ding et al. (2005), Xu et al. (2013); E–W extensional graben in South Tibet (ST) after Lee et al. (2011) and India/Asia collision after Ding et al. (2005) and references therein. Exhumation of CTP, GB, and GH after Rohrmann et al. (2012), Dai et al. (2013), Wang et al. (2010) and Xu et al. (2013). THTS, Tethyan Himalaya Thrust system; CTP, central Tibetan Plateau; GB, Gangdese belt; TH, Tethyan Himalaya; GH, Greater Himalaya. Exhumation events shown in light grey hatching lines are based on the Ar–Ar data, while those shown in grey are based on FT, U–Th/He data.

Miocene, heralded the development of the main modern river systems in south and north Tibet. Subsequently, tectonic and climatic interactions have continued to shape the Tibetan Plateau.

8. Conclusions

Low-temperature thermochronology data from northern Tethyan Himalayan sequences and the Indus Yarlung suture zone in the Zedang area, southeast Tibet, reveal two cooling episodes: one during the Eocene and another commencing in middle Miocene. These resulted from different histories of exhumation and regional erosion in south Tibet. Since the India–Asia collision, a south-vergent imbricate Tethyan Himalayan fold–thrust system has developed in Tethyan Himalaya, resulting in an Eocene–Oligocene cooling event in south Tibet. A later cooling event related to activity of the GCT in the Luobusha area commenced in early Miocene. However, the main rapid cooling episode commencing in middle Miocene in Zedang probably as resulting from incision of branches of the Yarlung–Zangbo River in this area. Further rapid cooling commencing at ca. 5 Ma in the Luobusha area and Yardoi dome may indicate the onset of activity of the Cona Graben in this area. These results support the notion that the Tibetan Plateau formed from a central 'core', which subsequently extended to the north and south.

Acknowledgements

Funding for this research was provided by the Australia Research Council DECRA (Discovery Early Career Research Award, DE120102245), and the Geological Survey Project of China (No. 1212011121275). The University of Melbourne thermochronology laboratory receives infrastructure support under the AuScope Program of NCRIS. We are grateful to Abaz Alimanovic and Christian Seiler for assistance with AFT, ZHe and AHe dating and Hanwen Dong for help with fieldwork. We thank Marc Jolivet, An Yin and previous anonymous reviewers, whose careful and thorough comments significantly improved this paper.

References

Aikman, A.B., Harrison, T.M., Herman, J., 2012. Age and thermal history of Eo- and Neohimalayan granitoids, eastern Himalaya. J. Asian Earth Sci. 51 (0), 85–97.
Aitchison, J.C., Badengzhu, Davis, A.M., Liu, J.B., Luo, H., Malpasa, J.G., McDermid, I.R.C., Wu, H., Ziabrev, S.V., Zhou, M., 2000. Remnants of a Cretaceous intra-oceanic subduction system within the Yarlung–Zangbo suture (south Tibet). Earth Planet. Sci. Lett. 183, 231–244.
Aitchison, J.C., Davis, A.M., Badengzhu, Luo, H., 2003. The Gangdese thrust: a phantom structure that did not raise Tibet. Terra Nova 15 (3), 155–162.
Bachmann, O., Oberli, F., Dungan, M., Meier, M., Mundil, R., Fischer, H., 2007. $^{40}Ar/^{39}Ar$ and U–Pb dating of the Fish Canyon magmatic system, San Juan Volcanic field, Colorado: evidence for an extended crystallization history. Chem. Geol. 236 (1–2), 134–166. http://dx.doi.org/10.1016/j.chemgeo.2006.09.005.
Braun, J., Simon-Labric, T., Murray, K.E., Reiners, P.W., 2014. Topographic relief driven by variations in surface rock density. Nat. Geosci. 7, 534–540.
Burbank, D.W., Blythe, A.E., Putkonen, J., Pratt-Sitaula, B.A., Barros, A., Ojha, T.P., 2003. Decoupling of erosion and precipitation in the Himalayas. Nature 426, 652–655.
Bureau of Geology and Mineral Resources of Xizang Autonomous Region (BGMXAR), 1993. Regional Geology of Xizang (Tibet) Autonomous Region. Geological Publishing House, Beijing.
Burg, J.P., Chen, G.M., 1984. Tectonics and structural zonation of southern Tibet. Nature 311, 219–223.
Carrapa, B., Orme, D.A., DeCelles, P.G., Kapp, P., Cosca, M.A., Waldrip, R., 2014. Miocene burial and exhumation of the India–Asia collision zone in southern Tibet: response to slab dynamics and erosion. Geology 42 (5), 443–446. http://dx.doi.org/10.1130/G35350.1.

Chen, Z., Liu, Y., Hodges, K.V., Burchfiel, B.C., Royden, L.H., Deng, C., 1990. The Kangmar dome: a metamorphic core complex in southern Xizang (Tibet). Science 250 (4987), 1552–1556.
Chu, M.F., Chung, S.L., Song, B., Liu, D., O'Reilly, S.Y., Pearson, N.J., 2006. Zircon U–Pb and Hf isotope constraints on the Mesozoic tectonics and crustal evolution of southern Tibet. Geology 34, 745–748.
Chung, S.L., Chu, M.F., Ji, J.Q., O'Reilly, S.Y., Pearson, N.J., Liu, D.Y., Lee, T.Y., Lo, C.H., 2009. The nature and timing of crustal thickening in southern Tibet: geochemical and zircon Hf isotopic constraints from postcollisional adakites. Tectonophysics 477, 36–48.
Cina, S.E., Yin, A., Grove, M., Dubey, C.S., Shukla, D.P., Lovera, O.M., Kelty, T.K., Gehrels, G.E., Foster, D.A., 2009. Gangdese arc detritus within the eastern Himalayan Neogene foreland basin: implications for the Neogene evolution of the Yalu-Brahmaputra River system. Earth Planet. Sci. Lett. 285, 150–162.
Copeland, P., Harrison, T.M., Pan, Y., Kidd, W.S.F., Roden, M., Zhang, Y.Q., 1995. Thermal evolution of the Gangdese Batholith, southern Tibet: a history of episodic unroofing. Tectonics 14, 223–236.
Dai, J., Wang, C., Hourigan, J., Li, Z., Zhuang, G., 2013. Exhumation history of the Gangdese Batholith, Southern Tibetan Plateau: evidence from apatite and zircon (U–Th)/He thermochronology. J. Geol. 121 (2), 155–172.
Davis, A.M., Aitchison, J.C., Zhu, B.D., Luo, H., Sergei, Z., 2002. Paleogene island arc collision related conglomerates, Yarlung–Tsangpo suture zone Tibet. Sediment. Geol. 150, 247–273.
DeCelles, P.G., Quade, J., Kapp, P., Fan, M., Dettman, D.L., Ding, L., 2007. High and dry in central Tibet during the Late Oligocene. Earth Planet. Sci. Lett. 253, 389–401. http://dx.doi.org/10.1016/j.epsl.2006.11.001.
Ding, L., Kapp, P., Wan, X., 2005. Paleocene–Eocene record of ophiolite obduction and initial India–Asian collision, south central Tibet. Tectonics 24 (3). http://dx.doi.org/10.1029/2004TC001729 TC3001.
Ding, L., Xu, Q., Yue, Y.H., Wang, H., Cai, F., Li, S., 2014. The Andean-type Gangdese Mountains: paleoelevation record from the Paleocene–Eocene Linzhou Basin. Earth Planet. Sci. Lett. 392, 250–264.
Dubois-Côté, V., Hébert, R., Dupuis, C., Wang, C.S., Li, Y., Dostal, J., 2005. Petrological and geochemical evidence for the origin of the Yarlung Zangbo ophiolites, southern Tibet. Chem. Geol. 214, 265–286.
Dunkl, I., AntolÍn, B., Wemmer, K., Rantitsch, G., Kienast, M., Montomoli, C., Ding, L., Carosi, R., Appel, E., El Bay, R., Xu, Q., von Eynaten, H., 2011. Metamorphic evolution of the Tethyan Himalayan flysch in SE Tibet. Geol. Soc. Lond., Spec. Publ. 353 (1), 45–69.
Edwards, M.A., Harrison, T.M., 1997. When did the roof collapse? Late Miocene north–south extension in the High Himalaya revealed by Th–Pb monazite dating of the Khula Kangri granite. Geology 25, 543–546.
Edwards, M.A., Kidd, W.S.F., Li, J.X., Yu, Y.J., Clark, M., 1996. Multistage development of the southern Tibet detachment system near Khula Kangri: new data from Gonto La. Tectonophysics 260, 1–19.
Fang, A., Yan, Z., Liu, X.H., Tao, J.R., Li, J.L., Pan, Y.S., 2006. The age of the plant fossil assemblage in the Liuqu Conglomerate of southern Tibet and its tectonic significance. Prog. Nat. Sci. 16, 55–64.
Farley, K.A., Wolf, R.A., Silver, L.T., 1996. The effects of long alpha-stopping distances on (U–Th)/He ages. Geochim. Cosmochim. Acta 60 (21), 4223–4229.
Flowers, R.M., Ketcham, R.A., Shuster, D.L., Farley, K.A., 2009. Apatite (U–Th)/He thermochronometry using a radiation damage accumulation and annealing model. Geochim. Cosmochim. Acta 73, 2347–2365.
Galbraith, R.F., 1981. On statistical models for fission track counts. Math. Geol. 13, 471–488.
Gleadow, A., Green, D.P., Lovering, J., 1986. Confined fission track lengths in apatite: a diagnostic tool for thermal history analysis. Contrib. Mineral. Petrol. 94 (4), 405–415.
Guenthner, W.R., Reiners, P.W., Ketcham, R.A., Nasdala, L., Giester, G., 2013. Helium diffusion in natural zircon: radiation damage, anisotropy, and the interpretation of zircon (U–Th)/He thermochronology. Am. J. Sci. 313 (3), 145–198.
Guo, L., Zhang, J.J., Zhang, B., 2008. Structures, kinematics, thermochronology and tectonic evolution of the Ramba gneiss dome in the northern Himalaya. Prog. Nat. Sci. 18, 851–860.
Harrison, T.M., Copeland, P., Kidd, W.S.F., Yin, A., 1995. Raising Tibet. Science 255 (5052). http://dx.doi.org/10.1126/science.255.5052.1663 (Tectonics 14, 1663–1670).
Harrison, T.M., Yin, A., Grove, M., Lover, O.M., Ryerson, F.J., Zhou, X., 2000. The Zedong Window: a record of superposed Tertiary convergence in southeastern Tibet. J. Geophys. Res. 105, 19211–19230.
Hetzel, R., Dunkl, I., Haider, V., Strobl, M., von Eynatten, H., Ding, L., Frei, D., 2011. Peneplain formation in southern Tibet predates the India–Asia collision and plateau uplift. Geology 39, 983–986. http://dx.doi.org/10.1130/G32069.1.
Hodell, D.A., Woodruff, F., 1994. Variations in the strontium isotopic ratio of seawater during the Miocene: stratigraphic and geochemical implication. Paleoceanography 9 (3), 405–426.
Hodell, D.A., Mueller, P.A., Garrido, J.R., 1991. Variations in the strontium isotopic composition of seawater during the Neogene. Geology 19, 24–27.
Hodges, K.V., 2000. Tectonics of the Himalaya and southern Tibet from two perspectives. Geol. Soc. Am. Bull. 112, 324–350.
Jolivet, M., Roger, F., Arnaud, N., Brunel, M., Tapponnier, P., Seward, D., 1999. Histoire de l'exhumation de l'Altun Shan: indications sur l'âge de la subduction du bloc du Tarim sous le système de l'Altyn Tagh (Nord Tibet). CR Acad. Sci. Paris 329, 749–755.
Jolivet, M., Brunel, M., Seward, D., Xu, Z., Yang, J., Roger, F., Tapponnier, P., Malavieille, J., Arnaud, N., Wu, C., 2001. Mesozoic and Cenozoic tectonics of the northern edge of the Tibetan plateau: fission-track constraints. Tectonophysics 343 (1–2), 111–134.
Ketcham, R.A., 2005. Forward and inverse modeling of low-temperature thermochronometry data. Rev. Mineral. Geochem. 58, 275–314.
Ketcham, R.A., Carter, A., Donelick, R.A., Barbarand, J., Hurford, A.J., 2007. Improved measurement of fission track annealing in apatite using C-axis projection. Am. Mineral. 92, 789–798.
Klootwijk, C.T., Geem, J.S., Peirce, J.W., Smith, G.M., 1992. Neogene evolution of the Himalayan–Tibetan region: constraints from ODP site 758 northern ninetyeast ridge bearing on climate change. Palaeogeogr. Palaeoclimatol. Palaeoecol. 95, 95–1410.
Lee, J., Bradley, R., William, H., Dinklage, S., Wang, Y., Gans, P., Calvert, A., Wan, J.L., Chen, W., Blythe, Ann E., McClelland, W., 2000. Evolution of the Kangmar Dome, southern Tibet: structural, petrologic, and thermochronologic constraints. Tectonics 19 (5), 872–895.
Lee, J., Hager, C., Wallis, S.R., Stockli, D.F., Whitehouse, M.J., Aoya, M., Wang, Y., 2011. Middle to late Miocene extremely rapid exhumation and thermal reequilibration in the Kung Co rift, southern Tibet. Tectonics 30 TC2007.
Li, G.W., Liu, X.H., Alex, P., Wei, L.J., Liu, X.B., Huang, F.X., Zhou, X.J., 2010. In-situ detrital zircon geochronology and Hf isotopic analyses from Upper Triassic Tethys sequence strata. Earth Planet. Sci. Lett. 297, 461–470.
Li, J.Y., Yang, J.S., Ba, D.Z., Xu, X.Z., Meng, F.C., Li, T.F., 2012. Origin of different dunites in the Luobusha ophiolite. Tibet. Acta Petrol. Sin. 28 (6), 1829–1845 (in Chinese with English abstract).
Li, G.W., Sandiford, M., Liu, X.H., Xu, Z.Q., Wei, L.J., Li, H.Q., 2014. Provenance of Late Triassic sediments in central Lhasa terrane, Tibet and its implication. Gondwana Res. 25, 1680–1689.
Liu, G., Einsele, G., 1994. Sedimentary history of the Tethyan basin in the Tibetan Himalayas. Geol. Rundsch. 83, 32–61.
Ludwig, K.R., 2003. Berkeley Geochronology Center Special Publication No. 4.
Malpas, J., Zhou, M.F., Robinson, P.T., Reynolds, P.H., 2003. Geochemical and geochronological constraints on the origin and emplacement of the Yarlung Zangbo ophiolites, southern Tibet. Geol. Soc. Lond. Spec. Publ. 218, 191–206.
McDowell, F.W., McIntosh, W.C., Farley, K.A., 2005. A precise 40Ar–39Ar reference age for the Durango apatite (U–Th)/He and fission-track dating standard. Chem. Geol. 214 (3–4), 249–263.
Meesters, A.G., Dunal, T.J., 2002. Solving the production–diffusion equation for finite diffusion domains of various shapes: Part I. Implications for low-temperature (U–Th)/He thermochronology. Chem. Geol. 186, 333–344.
Molnar, P., England, P., Martinod, J., 1993. Mantle dynamics, uplift of the Tibetan Plateau, and the Indian monsoon. Rev. Geophys. 31, 357–396.
Nakayama, K., Ulak, P.D., 1999. Evolution of fluvial style in the Siwalik Group in the foothills of the Nepal Himalaya. Sediment. Geol. 125 (3), 205–224.
Quade, J., Breecker, D.O., Daeron, M., Eilter, J., 2011. The paleoaltimetry of Tibet: an isotopic perspective. Am. J. Sci. 311 (2), 77–115.
Quidelleur, X., Grove, M., Lovera, O.M., Harrison, T.M., Yin, A., Ryerson, F.J., 1997. Thermal evolution and slip history of the Renbu Zedong Thrust, southeastern Tibet. J. Geophys. Res. 102, 2659–2679.
Ratschbacher, L., Frisch, W., Liu, G.H., Chen, C.S., 1994. Distributed deformation in southern and western Tibet during and after the India–Asia collision. J. Geophys. Res. 99 (B10), 19917–919945.
Reiners, P.W., Spell, T.L., Nicolescu, S., Zanetti, K.A., 2004. Zircon (U–Th)/He thermochronometry: He diffusion and comparisons with $^{40}Ar/^{39}Ar$ dating. Geochim. Cosmochim. Acta 68 (8), 1857–1887.
Rohrmann, A., Kapp, P., Carrapa, B., Reiners, P.W., Guynn, J., Ding, L., Heizler, M., 2012. Thermochronologic evidence for plateau formation in central Tibet by 45 Ma. Geology 40, 187–190.
Rowley, D.B., Currie, B.S., 2006. Palaeo-altimetry of the late Eocene to Miocene Lunpola basin, central Tibet. Nature 439, 677–681. http://dx.doi.org/10.1038/nature04506.
Sobel, E.R., Schoenbohm, L.M., Jie, Chen, Thiede, R., Stockli, D.F., Sudo, M., Strecke, M.R., 2011. Late Miocene–Pliocene deceleration of dextral slip between Pamir and Tarim: implications for Pamir orogenesis. Earth Planet. Sci. Lett. 304 (3–4), 369–378.
Spicer, R.A., Harris, N.B.W., Widdowson, M., Herman, A.B., Guo, S., Valdes, P.J., Wolfe, J.A., Kelley, S.P., 2003. Constant elevation of southern Tibet over the past 15 million years. Nature 421, 622–624. http://dx.doi.org/10.1038/nature01356.
Stockli, D.F., Taylor, M., Yin, A., Harrison, T.M., D'Andrea, J., Kapp, P., Ding, L., 2002. Late Miocene–Pliocene inception of E–W extension in Tibet as evidenced by apatite (U–Th)/He data. Geol. Soc. Am. Abstr. Programs 34, 411.
Sun, X., Wang, P., 2005. How old is the Asian monsoon system? Palaeobotanical records from China. Palaeogeogr. Palaeoclimatol. Palaeoecol. 222, 181–222.
Tapponnier, P., Xu, Z.Q., Roger, F., Meyer, B., Arnaud, N., Wittlinger, G., Yang, J.S., 2001. Oblique stepwise rise and growth of the Tibet Plateau. Science 294, 1671–1677.
Tian, Y., Kohn, B.P., Zhu, C.Q., Xu, M., Hu, S.B., Gleadow, A.J.W., 2012. Post-orogenic evolution of the Mesozoic Micang Shan Foreland Basin system, central China. Basin Res. 24, 70–90. http://dx.doi.org/10.1111/j.1365-2117.2011.00516.x.
Tian, Y., Kohn, B.P., Gleadow, A.J.W., Hu, S., 2013. Constructing the Longmen Shan eastern Tibetan Plateau margin: insights from low-temperature thermochronology. Tectonics 32, 576–592. http://dx.doi.org/10.1002/tect.20043.
Tian, Y., Kohn, B.P., Gleadow, A.J.W., Hu, S., 2014. A thermochronological perspective on the morphotectonic evolution of the southeastern Tibetan Plateau. J. Geophys. Res. Solid Earth 119. http://dx.doi.org/10.1002/2013JB010429.
Vermeesch, P., 2009. RadialPlotter: a Java application for fission track, luminescence and other radial plots. Radiat. Meas. 44 (4), 409–410.
Wang, C., Zhao, X., Liu, Z.F., Lippert, P.C., Graham, S.A., Coe, R.S., Yi, H., Zhu, L.D., Liu, S., Li, Y.L., 2008. Constraints on the early uplift history of the Tibetan Plateau. Proc. Natl. Acad. Sci. 105 (13), 4987–4992.
Wang, A., Garver, J., Wang, G., Smith, J.A., Zhang, K., 2010. Episodic exhumation of the Greater Himalayan Sequence since the Miocene constrained by fission track thermochronology in Nyalam, central Himalaya. Tectonophysics 495, 315–323.
Wang, J., Hu, X.-M., Garzanti, E., Wu, F., 2013. Upper Oligocene–Lower Miocene Gangrinboche Conglomerate in the Xigaze Area, Southern Tibet: implications for Himalayan Uplift and Paleo–Yarlung–Zangbo initiation. J. Geol. 121 (4), 425–444.

Wei, L.J., Liu, X.H., Yan, F.H., Mai, X.S., Li, G.W., Liu, X.B., Zhou, X.J., 2011. Palynological evidence sheds new light on the age of the Liuqu Conglomerates in Tibet and its geological significance. Sci. China Earth Sci. 54, 901–911.
Wu, Z.H., Zhang, Y.S., Hu, D.G., Zhao, X.T., Ye, P.S., 2008. The Quaternary normal faulting of the Cona-Oiga Rift. Seismol. Geol. 30 (1), 144–160 (Chinese with English abstract).
Xu, Z., Wang, Q., Pêcher, A., Liang, F., Qi, X., Cai, Z.H., Li, H.Q., Zeng, L.S., Cao, H., 2013. Orogen-parallel ductile extension and extrusion of the Greater Himalaya in the late Oligocene and Miocene. Tectonics 32, 191–215.
Xu, Z., Dilek, Y., Yang, J.S., Liang, F.H., Liu, F., Badengzhu, Cai, Z.H., Li, G.W., Dong, H.W., 2015. Crustal structure of the Indus–Tsangpo Suture Zone and its ophiolites, southern Tibet. Gondwana Res. 27 (2), 502–524.
Yin, A., 2006. Cenozoic evolution of the Himalayan Orogen as constrained by alongstrike variations of structural geometry, exhumation history, and foreland sedimentation. Earth Sci. Rev. 76, 1–134.
Yin, A., Harrison, T.M., 2000. Geologic evolution of the Himalayan–Tibetan orogen. Annu. Rev. Earth Planet. Sci. 28, 211–280.
Yin, A., Harrison, T.M., Ryerson, F.J., Chen, W.J., Kidd, W.S.F., Copeland, P., 1994. Tertiary structural evolution of the Gangdese Thrust system, southeastern Tibet. J. Geophys. Res. 99, 18175–18201.
Yin, A., Harrison, T.M., Murphy, M.A., Grove, M., Nie, S., Ryerson, F.J., Wang, X.F., Chen, Z.L., 1999. Tertiary deformation history of southeastern and southwestern Tibet during the Indo-Asian collision. Geol. Soc. Am. Bull. 111, 1–21.
Zeng, L., Gao, L.E., Xie, K., Liu-Zeng, J., 2011. Mid-Eocene high Sr/Y granites in the Northern Himalayan gneiss domes: melting thickened lower continental crust. Earth Planet. Sci. Lett. 303 (3), 251–266.
Zhang, J., Santosh, M., Wang, X., Guo, L., Yang, X., Zhang, B., 2012. Tectonics of the northern Himalaya since the India–Asia collision. Gondwana Res. 21 (4), 939–960.
Zhao, Z.D., Mo, X.X., Dilek, Y., Niu, Y.L., DePaolo, D.J., Robinson, P., Zhu, D.C., 2009. Geochemical and Sr–Nd–Pb–O isotopic compositions of the postcollisional ultrapotassic magmatism in SW Tibet: petrogenesis and implications for India intra-continental subduction beneath southern Tibet. Lithos 113, 190–212.
Zhu, D.C., Zhao, Z.D., Niu, Y.L., Dilek, Y., Hou, Z.Q., Mo, X.X., 2013. The origin and pre-Cenozoic evolution of the Tibetan Plateau. Gondwana Res. 23, 1429–1454.